Effect of input–output coupling on the sensitivity of coupled resonator optical waveguide gyroscopes

Dmitriy Kalantarov and Christopher P. Search*

Department of Physics and Engineering Physics, Stevens Institute of Technology, Castle Point on Hudson, Hoboken, New Jersey 07030, USA
**Corresponding author: csearch@stevens.edu*

Received September 27, 2012; revised December 19, 2012; accepted December 20, 2012; posted December 20, 2012 (Doc. ID 177003); published January 22, 2013

We analyze how the evanescent coupling, κ_e, between the outermost resonators and input/output waveguides of an N-resonator coupled resonator optical waveguide (CROW) gyroscope affects the transmission and sensitivity to rotations. For constant coupling between resonators κ, rotation sensitivities increase as both $\kappa_e \to 0$ and $\kappa_e \to 1$ while between these two limits the sensitivity has a minimum. In the weak coupling regime, $\kappa_e \to 0$, the sensitivity is enhanced by Fabry–Perot oscillations due to the impedance mismatch at the input/output waveguide–CROW interface, while in the strong coupling regime, $\kappa_e \to 1$, the sensitivity is reduced because the outermost resonators no longer contribute to the CROW transmission. For small N the sensitivity is proportional to N^2, while at larger N the sensitivity begins to decrease due to resonator losses.

OCIS codes: 060.2800, 120.5790, 130.3120.

1. INTRODUCTION

Coupled resonator optical waveguides (CROWs) are an array of optical microresonators sequentially coupled by nearest-neighbor evanescent fields [1–3]. In an infinite CROW, the periodic structure leads to the creation of energy bands with group velocities controllable by the evanescent coupling between resonators. The tunability of both the group velocity and bandwidth of the transmission bands by evanescent coupling has caused CROWs to emerge as a promising technology for applications in integrated photonic circuits, such as optical delay lines, buffers, optical filters, and nonlinear optics [3]. However, infinite-length CROWs are a mathematical idealization, and in reality CROWs have a finite number of resonators that must be coupled to the outside world via evanescent coupling to input and output optical waveguides, as illustrated in Fig. 1. The termination and coupling of the CROW array to waveguides not only interrupts the periodicity of the resonator array but also results in an impedance mismatch due to the differing structure of the waveguides [3]. This impedance mismatch leads to reflections at the waveguide–CROW resonator interface that appear as ripples in the transmission band [3–6]. These ripples, which are equal to the number of resonators N in the CROW, have been referred to as Fabry–Perot (FP) oscillations, since the impedance mismatch creates an effective FP resonator enclosing the CROW [5,6].

More recently, it has been shown that CROWs hold great promise as micro-optical gyroscopes with navigation-grade sensitivities [7–15]. This is part of a growing interest in the development of microphotonic integrated optical gyroscopes that have sensitivities exceeding micro-electromechanical gyroscopes for portable applications such as handheld navigation in global positioning system denied regions [16]. In a CROW, the evanescent coupling between resonators is characterized by the coupling constant κ such that $1/2\kappa$ is the average number of times a photon will circulate around a resonator before jumping to one of the neighboring resonators. Weak coupling $\kappa \ll 1$ between resonators causes light to circulate multiple times within each resonator, and with each successive round trip the rotation-induced phase shift increases. The phase difference between clockwise and counterclockwise propagating waves in each resonator due to the Sagnac effect is therefore multiplied by the number of round-trips $1/2\kappa$ [8,9]. While phase enhancement due to multiple round trips also occurs in resonant fiber-optic gyroscopes (RFOGs) consisting of a single optical fiber resonator, CROWs add to this distributed interference between resonators that further enhances the phase sensitivity to rotations. In particular, the alternating sign of the rotation-induced Sagnac phase between adjacent resonators leads to the formation of a bandgap in the transmission that is a sensitive measure of the Sagnac phase [9].

This paper will show the importance of the waveguide–CROW coupling to the overall response and sensitivity of an N-resonator CROW gyroscope. Previous discussions of CROW gyroscopes have ignored the role of the FP oscillations in the rotation sensitivity, which we will show here to be as important as the intraresonator Sagnac effect emphasized in [8]. As the coupling between the waveguides and outermost resonators of the CROW is reduced toward zero, thereby increasing the finesse of the effective CROW FP resonator, the rotation sensitivity of the gyroscope is significantly increased. By contrast, in the opposite limit of strong coupling to the waveguides, the sensitivity also increases as the coupling increases, albeit by a smaller amount, since in this regime the outermost resonators no longer contribute to the CROW transmission. In between these two limits, at moderate waveguide–resonator coupling, the gyroscope sensitivity has a minimum. We also show here that the sensitivity of the CROW gyroscope increases as $(N+1)^2$ until resonator losses become large enough to reduce the sensitivity for further increases in the number of resonators. These results

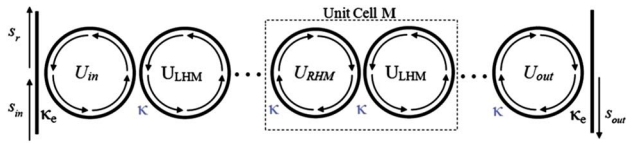

Fig. 1. (Color online) Microring CROW gyroscope showing the relationship between the resonators, transfer matrices, and repetitive unit cell defined in the text. s_{in} and s_{out} are the input signal and transmitted field, respectively, such that $T(\phi_S) = |s_{\text{out}}/s_{\text{in}}|^2$. Based on the propagation direction of s_{out} in the figure, the number of resonators must be odd due to phase matching.

have broader applicability to CROWs, since little attention has been paid to the FP oscillations except to minimize them in order to produce smooth transmission bands, such as by apodization of the couplings [17].

2. MODEL

The CROW gyroscope we will consider is illustrated in Fig. 1, consisting of a linear array of circular ring-shaped microresonators of radius R coupled to input and output waveguides. When the CROW is rotated about an axis perpendicular the plane of the device, the Sagnac effect leads to a nonreciprocal phase shift for waves of frequency ω propagating in the clockwise [right-handed mode (RHM) in Fig. 1] and counterclockwise [left-handed mode (LHM) in Fig. 1] direction around each resonator. Assuming a clockwise inertial rotation Ω about an axis perpendicular to the plane of the resonators, the clockwise propagating wave acquires upon one full revolution around a resonator the Sagnac phase ϕ_S, while the counterclockwise wave acquires the phase $-\phi_S$, where

$$\phi_S = 2\pi\omega\Omega R^2/c^2. \tag{1}$$

To analyze the transmission through the rotating CROW, we utilize the transfer matrix [17,18] approach developed in [10,11]. As a result of momentum conservation, the propagating RHM of one resonator couples to the counterpropagating LHM of the adjacent resonator and vice versa. Consequently, transmission can be expressed in terms of input (U_{in}), output (U_{out}), LHM (U_{LHM}), and RHM (U_{RHM}) transfer matrices [10,11]:

$$U_{\text{in}} = \frac{i}{\sqrt{\kappa_e}}\begin{pmatrix} e^{i(\phi_p+\phi_S/2)} & -\sqrt{1-\kappa_e}e^{i(\phi_p+\phi_S/2)} \\ \sqrt{1-\kappa_e}e^{-i(\phi_p+\phi_S/2)} & -e^{-i(\phi_p+\phi_S/2)} \end{pmatrix}, \tag{2}$$

$$U_{\text{out}} = \frac{1}{\sqrt{\kappa_e}}\begin{pmatrix} e^{i(\phi_p+\phi_S/2)} & -\sqrt{1-\kappa_e}e^{i(\phi_p+\phi_S/2)} \\ \sqrt{1-\kappa_e}e^{-i(\phi_p+\phi_S/2)} & -e^{-i(\phi_p+\phi_S/2)} \end{pmatrix} \times \begin{pmatrix} \frac{\sqrt{1-\kappa}}{\sqrt{\kappa}} & \frac{1}{\sqrt{\kappa}} \\ \frac{1}{\sqrt{\kappa}} & \frac{-\sqrt{1-\kappa}}{\sqrt{\kappa}} \end{pmatrix}, \tag{3}$$

$$U_{\text{RHM}} = \frac{i}{\sqrt{\kappa}}\begin{pmatrix} \sqrt{1-\kappa}e^{i(\phi_p+\phi_S/2)} & -e^{i(\phi_p+\phi_S/2)} \\ e^{-i(\phi_p+\phi_S/2)} & -\sqrt{1-\kappa}e^{-i(\phi_p+\phi_S/2)} \end{pmatrix}, \tag{4}$$

$$U_{\text{LHM}} = \frac{-i}{\sqrt{\kappa}}\begin{pmatrix} \sqrt{1-\kappa}e^{i(\phi_p-\phi_S/2)} & -e^{i(\phi_p-\phi_S/2)} \\ e^{-i(\phi_p-\phi_S/2)} & -\sqrt{1-\kappa}e^{-i(\phi_p-\phi_S/2)} \end{pmatrix}, \tag{5}$$

where $\phi_p = \beta\pi R$ is the propagation phase for the resonator with $\beta = \omega n/c - ia/2$ with effective index of refraction n. $a = (n\omega/c)Q_{\text{int}}^{-1}$ is the power attenuation coefficient per unit length expressed in terms of the intrinsic (unloaded) Q factor Q_{int} of the resonator [10,19]. For convenience we will always assume that $2\pi\omega nR/c = 2\pi m$, corresponding to the mth azimuthal resonator mode, so that the real part of the optical propagation phase can be ignored. This corresponds to choosing ω to be in the center of one of the CROW transmission bands. (Note that in all of our results we have used a signal wavelength of $\lambda = 2\pi c/\omega = 1.55$ μm.) The opposite signs of the Sagnac phases in U_{RHM} and U_{LHM} are due to the different signs of the Sagnac phase for clockwise and counterclockwise waves relative to the rotation Ω. κ is the dimensionless power coupling between resonators and κ_e is the coupling between first (last) resonators and the external waveguides. Because of conservation of energy, $0 \le \kappa, \kappa_e \le 1$.

The coupled cavity waveguide transmission matrix for a signal propagating from the left-to-right waveguide is

$$T_{\text{CCW}} = U_{\text{out}}(U_{\text{LHM}}U_{\text{RHM}})^M U_{\text{LHM}}U_{\text{in}} = \begin{pmatrix} T_{11} & T_{12} \\ T_{21} & T_{22} \end{pmatrix}, \tag{6}$$

where $M = (N-3)/2$. Furthermore, we can simplify the unit cell translation matrix $\mathcal{T} = (U_{\text{LHM}}U_{\text{RHM}})$ via the Chebyshev polynomials of the second kind, $u_J(x)$ [20]:

$$\mathcal{T}^M = \begin{pmatrix} Au_{M-1}(x) - u_{M-2}(x) & Bu_{M-1}(x) \\ B^*u_{M-1}(x) & A^*u_{M-1}(x) - u_{M-2}(x) \end{pmatrix}. \tag{7}$$

$A = (1 - e^{-2i\phi} - \kappa)/\kappa$, $B = \sqrt{1-\kappa}(e^{-2i\phi} - 1)/\kappa$, and $x = (1 - \kappa - \cos(2\phi))/\kappa$. The transmission function, which is proportional to the output power, is $T(\phi_S) = 1/|T_{22}|^2$.

The gyroscope scale factor, S, which measures the sensitivity to rotations, relates the change in the transmission to a small change in the inertial rotation rate, $\delta T = S\delta\Omega$, and is expressed as

$$S = dT/d\Omega = (2\pi\omega R^2/c^2)(dT/d\phi_S). \tag{8}$$

As with a conventional fiber-optic gyroscope, one desires to measure rotations where the slope $dT/d\phi_S$ is a maximum and the response is linear. In practice, $\pi\omega nR/c$ could be used to phase bias $T(\phi_S)$ to center regions of maximal transmission slope around $\phi_S \approx 0$. Note that the shot-noise-limited minimum rotation rate can be easily calculated directly from the maximum value of the scale factor:

$$\Omega_{\text{min}} = \frac{\pi}{2S_{\text{max}}}\sqrt{\frac{hc\Delta f}{\lambda\eta P_{\text{opt}}}}, \tag{9}$$

where Δf is the measurement bandwidth, P_{opt} is the detected optical power, and η is the quantum efficiency of the photodetector [16].

3. RESULTS

The central feature of this paper is that for fixed κ, there exist two regimes for the scale factor in the interval $0 \le \kappa_e \le 1$, as depicted in Fig. 2, which shows the maximum transmission slope $(dT/d\phi_S)_{\text{max}}$. For increasing κ_e, the transmission slope first decreases and then reaches a minimum, at which point it begins to increase again as $\kappa_e \to 1$. We define the two regimes

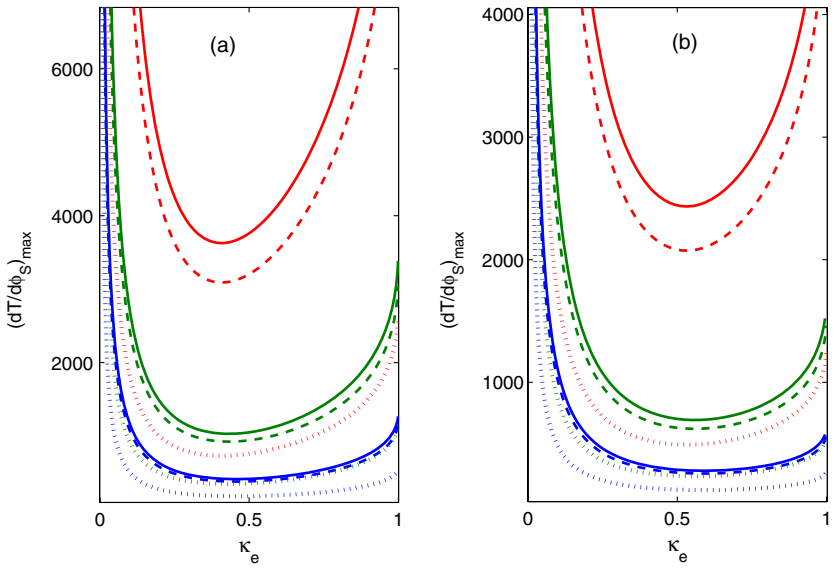

Fig. 2. (Color online) Maximum transmission slope $(dT/d\phi_S)_{\max}$ for $N = 11$ (blue curves), 15 (green curves), and 23 (red curves) resonators as a function of κ_e for (a) $\kappa = 0.05$ and (b) $\kappa = 0.1$. Solid curves represent lossless resonators ($Q_{\text{int}}^{-1} = 0$), dashed curves are $Q_{\text{int}} = 10^6$, and dotted curves are $Q_{\text{int}} = 10^5$. The resonator mode number in all cases is $m = 162$ for $R = 11.5$ μm Si resonators. For each of the three line styles, red curves are the topmost, green curves are in the middle, and blue are on the bottom.

as the weak coupling regime for κ_e values to the left of the minimum of $(dT/d\phi_S)_{\max}$ and the strong coupling regime for κ_e values to the right of the minimum. As can be seen in Fig. 3, the maximum slope of the transmission always occurs at the edges of the transmission band and yields the maximum scale factor $S_{\max}$. The transmission band ripples are due to the effective FP resonator formed by the coupling of the CROW array to the input/output waveguides with finesse $\mathcal{F} \sim 2\pi/\kappa_e$. As $\kappa_e \to 0$, the depth and slope of the transmission band ripples increase in a manner similar to the change in the transmission resonances of a FP resonator with increasing finesse.

In the weak coupling regime, for a given κ_e, the maximum slope increases as $(dT/d\phi_S)_{\max} \propto (N+1)^2/\kappa_e$, which is shown in Fig. 4. A similar quadratic dependence has been predicted for the sensitivity of an atom gyroscope consisting of a chain of coupled ring-shaped atom interferometers, and it is due to the slope of the Chebyshev polynomials $u_J(x)$ at the limits $x \to \pm 1$, which correspond to the transmission band edges [20]. This sensitivity, which is linear in the rotation Ω, is in contrast to the maximum sensitivity indicated in [8], $S_{\max} = (4\pi\omega R^2/c^2)(N+1)/\kappa$, from which it was argued that a CROW gyro was no more sensitive than a RFOG with enclosed area $(N+1)\pi R^2$. While this N^2 dependence of the

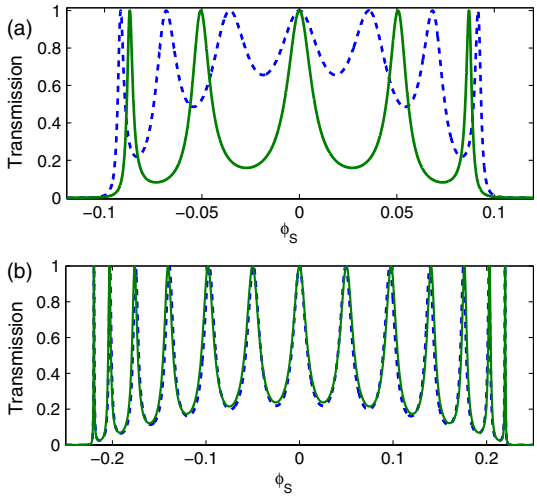

Fig. 3. (Color online) (a) Transmission spectra of an $N = 7$ gyro for $\kappa_e = 0.1$ (blue dashed curve) and $\kappa_e = 0.61$ (green solid curve). In both cases $\kappa = 0.01$, and they have identical maximum slopes $(dT/d\phi_S)_{\max} = 417.6$. (b) Transmission spectra of an $N = 13$ CROW gyro with $\kappa_e = 0.107$ (blue dashed curve) and $N = 15$ with $\kappa_e = 0.843$ (green solid curve). Both have $\kappa = 0.05$ and $(dT/d\phi_S)_{\max} = 1719$. These results are for lossless resonators.

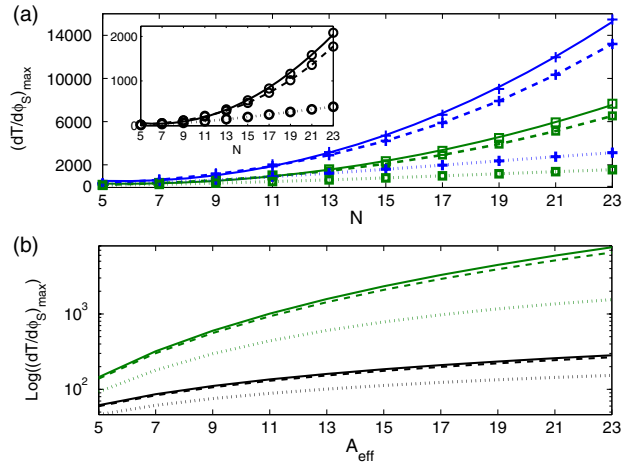

Fig. 4. (Color online) (a) $(dT/d\phi_S)_{\max}$ versus N in the weak coupling and strong coupling (inset) regime. Data markers are numerically calculated slopes, while curves are quadratic fits, $(dT/d\phi_S)_{\max} = \alpha + \beta N^2$. Blue curves with crosses are $\kappa_e = 0.05$, while green curves with squares are $\kappa_e = 0.1$. Inset shows $\kappa_e = 0.95$. In all cases $\kappa = 0.1$ and the microresonator mode number is $m = 162$, assuming $R = 11.5$ μm Si resonators. (b) $\log((dT/d\phi_S)_{\max})$ comparing an N-ring CROW to a single resonator RFOG with equal enclosed geometric area $A_{\text{eff}} = N\pi R^2$. Green curves (top three curves) are for the CROW with $\kappa = \kappa_e = 0.1$, and black curves (bottom three curves) are the RFOG with waveguide–resonator coupling $\kappa_e = 0.1$. In both (a) and (b), solid curves represent lossless resonators, dashed curves are $Q_{\text{int}} = 10^6$, and dotted curves are $Q_{\text{int}} = 10^5$.

scale factor is ultimately attributable to the periodicity of the CROW, which leads to the formation of transmission bands and bandgaps, the waveguide coupling further modulates this slope by increasing the number of round trips light makes in the array. With each additional round trip, the transmission slopes at both the band edges and transmission band ripples increase because of the multiple interferences.

In the presence of resonator losses, represented by an intrinsic Q factor Q_{int} of the resonators, signal attenuation leads to lowering of the transmission slopes and, hence, the scale factor. The effective length of the CROW is determined by the resonator couplings, since the electric field circulates $\sim 1/2\kappa$ times around each resonator before transmitting to a neighboring resonator with the factor of 1/2, due to the fact that each resonator is evanescently coupled at two points. Including both of the waveguide couplings, this yields a total path length $L_{\text{eff}} = \pi R(2\kappa_e^{-1} + (N-1)\kappa^{-1})$. This reduces down to the definition of the effective length of a CROW given in [8,19] for $\kappa_e = \kappa$ and $N \gg 1$. Intrinsic losses lead to an exponential reduction in the transmission by an amount $\exp(-aL_{\text{eff}}) = \exp(-L_{\text{eff}}\omega n/cQ_{\text{int}})$. For realistic rotation rates, this attenuation is independent of the inertial rotation, so that the maximum transmission slope scales as

$$\left(\frac{dT}{d\phi_S}\right)_{\max} \propto \frac{(N+1)^2}{\kappa_e} e^{-\omega n L_{\text{eff}}/cQ_{\text{int}}} = \frac{(N+1)^2}{\kappa_e} e^{-\left(\frac{N-1}{\kappa}+\frac{2}{\kappa_e}\right)\frac{m\pi}{Q_{\text{int}}}}. \tag{10}$$

Included in Figs. 2 and 4 is the effect of finite Q factors on the maximum transmission slope, from which one can see that the overall shape of the curves remains the same and they are simply shifted down toward a lower sensitivity. However, Eq. (10) implies that as N increases there should be a point given by $\omega n L_{\text{eff}}/cQ_{\text{int}} \sim 1$ where the exponential losses begin to dominate the quadratic growth in the sensitivity, leading to a decrease in the sensitivity for further increases in N. This transition begins to occur in Fig. 4(a) for $Q_{\text{int}} = 10^5$ at $N \approx 20$, as shown by the flattening of the parabola. Figure 5(a) shows the sensitivity versus N for a smaller Q factor, where it can be clearly seen that the sensitivity reaches a maximum, after which it begins to decrease. As a further confirmation of the dependence of $S_{\max}$ on Q_{int}, Fig. 5 shows a linear decrease in $\log((dT/d\phi_S)_{\max})$ with Q_{int}^{-1} with slope proportional to $(N-1)\kappa^{-1} + 2\kappa_e^{-1}$. We note that resonators with Q factors of at least 10^5 are readily fabricated using silicon-on-insulator resonators [21].

As N increases, the maximum slope in the strong coupling regime begins to strongly mimic the weak coupling regime, with $(dT/d\phi_S)_{\max}$ versus κ_e approaching a symmetric parabola with a larger curvature and minimum value, which is a reflection of the decreasing importance of edge effects as $N \to \infty$. However, for finite $N \approx 10$, $S_{\max}$ is much smaller in the limit $\kappa_e \to 1$ in comparison to $\kappa_e \to 0$. Furthermore, the value for which the CROW gyro enters the strong coupling regime is not constant: in Fig. 6, it can be seen that the location of the minimum $(dT/d\phi_S)_{\max}$ occurs at approximately $(\kappa_e)_{\min} = \sqrt{\kappa} + \frac{1}{\sqrt{N+1}}$, which is the coupling that minimizes the FP oscillations in the transmission band. This minimum is independent of Q_{int}, since losses do not depend on ϕ_S.

From Fig. 2 there are two values of κ_e, one in the weak and one in the strong coupling regime, with identical maximum

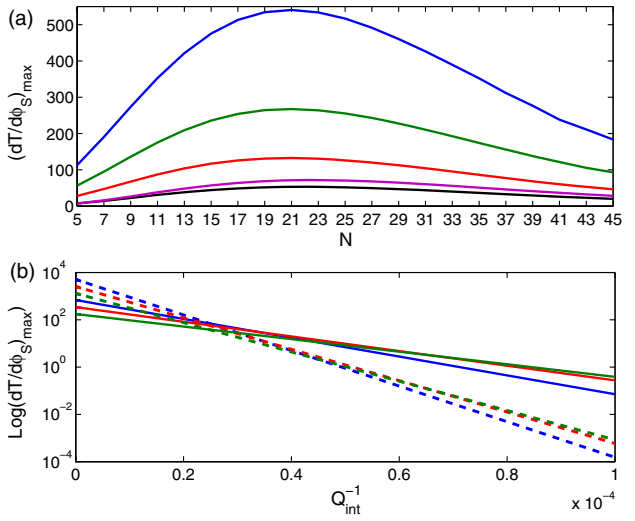

Fig. 5. (Color online) (a) $(dT/d\phi_S)_{\max}$ versus N for $Q_{\text{int}} = 4.75 \times 10^4$, showing a decrease in sensitivity for large N. For all curves $\kappa = 0.1$ and the mode number is $m = 162$, while the waveguide couplings of the curves from topmost to bottommost curve in descending order are $\kappa_e = 0.05$ (blue curve), $\kappa_e = 0.1$ (green curve), $\kappa_e = 0.2$ (red curve), $\kappa_e = 0.7$ (purple curve), and $\kappa_e = 0.95$ (black curve). (b) $\log((dT/d\phi_S)_{\max})$ versus Q_{int}^{-1} for $N = 7$ and 15, showing a linear decrease in sensitivity with increasing Q_{int}^{-1}. Blue curves are $\kappa_e = 0.05$, red curves are $\kappa_e = 0.1$, and green curves are $\kappa_e = 0.2$. Solid curves are $N = 7$, while dashed curves are $N = 15$. Note that at $Q_{\text{int}}^{-1} = 0$ the curves in descending order from topmost to bottommost are $\kappa_e = 0.05$, $N = 15$, $\kappa_e = 0.1$, $N = 15$, $\kappa_e = 0.2$, $N = 15$, $\kappa_e = 0.05$, $N = 7$, $\kappa_e = 0.1$, $N = 7$, and $\kappa_e = 0.2$, $N = 7$.

slopes. Plotting in Fig. 3(a) both transmissions for $N = 7$ and $Q_{\text{int}}^{-1} = 0$ with $(dT/d\phi_S)_{\max} = 417.6$, it is seen that in the weak coupling regime the system acts as a normal seven-resonator CROW based on the number of transmission band ripples, while in the strong coupling regime, it responds as if it were a five-resonator CROW, with the outermost ripples having completely disappeared. More generally, in the weak coupling regime the system acts as an N-resonator CROW gyro, while in the strong coupling regime it responds as an $N-2$-resonator CROW gyro. This is understood by noting that the power coupling rate between the resonators and the waveguides is $\Gamma \approx \kappa_e \nu_{\text{FSR}}$. The transmission resonances disappear as $\kappa_e \to 1$, because their line width approaches

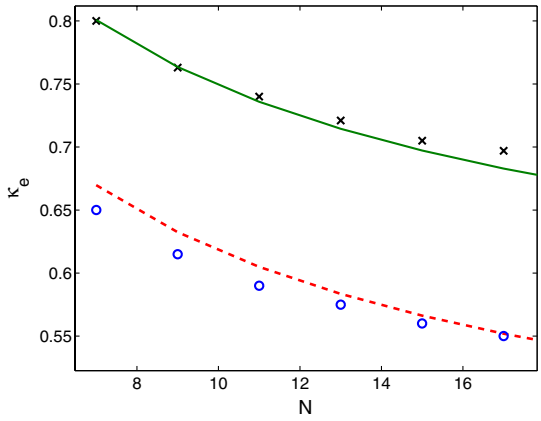

Fig. 6. (Color online) κ_e value at which the sensitivity $(dT/d\phi_S)_{\max}$ is a minimum versus resonator number N for $\kappa = 0.1$ (circles) and $\kappa = 0.2$ (x's). The red dashed and green solid curves are the fit $(\kappa_e)_{\min} = \sqrt{\kappa} + \frac{1}{\sqrt{N+1}}$. This was calculated for lossless resonators, but the results are unchanged when losses are included.

the free spectral range of the resonator ν_{FSR}. As a corollary to the above conclusion, one can show that for a particular κ_e in the strong coupling regime of an $N+2$ system, there exists a weak coupling κ_e of an N-resonator CROW gyro having a virtually identical transmission spectrum, as depicted in Fig. 3(b). Because of the N^2 dependence of $S_{\max}$, this effective reduction in the number of resonators reduces the sensitivity and partly explains the asymmetry in maximum sensitivities between weak and strong couplings seen in Fig. 2.

4. CONCLUSIONS

In conclusion, we have examined the effect of waveguide–resonator coupling, κ_e, on the sensitivity of a CROW gyroscope. By decreasing the coupling at the waveguide–CROW interface, the rotation sensitivity can be increased by a factor of $(N+1)^2/\kappa_e$ due to a narrowing of the FP oscillations in the transmission band that are a result of interference between multiple reflections. This implies that a factor of N fewer resonators are needed to achieve a desired rotation sensitivity than had been predicted before [8]. By contrast, for strong coupling to the waveguides, the sensitivity is reduced, not only because of broader FP oscillations but also because of a reduction in the effective enclosed geometric area of the gyroscope from $N(\pi R^2)$ to $(N-2)(\pi R^2)$. Furthermore we have shown that for small CROW arrays, intrinsic resonator losses do not affect the N^2 dependence of the sensitivity, while for larger N values one observes a reduction in the sensitivity for further increases in N.

REFERENCES

1. A. Yariv, Y. Xu, R. K. Lee, and A. Scherer, "Coupled-resonator optical waveguide: a proposal and analysis," Opt. Lett. **24**, 711–713 (1999).
2. F. Xia, L. Sekaric, M. O'Boyle, and Y. Vlasov, "Coupled resonator optical waveguides based on silicon-on-insulator photonic wires," Appl. Phys. Lett. **89**, 041122 (2006).
3. F. Morichetti, C. Ferrari, A. Canciamilla, and A. Melloni, "The first decade of coupled resonator optical waveguides: bringing slow light to applications," Laser Photon. Rev. **6**, 74–96 (2012).
4. P. Chak and J. E. Sipe, "Minimizing finite-size effects in artificial resonance tunneling structures," Opt. Lett. **31**, 2568–2570 (2006).
5. Y.-H. Ye, J. Ding, D.-Y. Jeong, I. C. Khoo, and Q. M. Zhang, "Finite-size effect on one-dimensional coupled-resonator optical waveguides," Phys. Rev. E **69**, 056604 (2004).
6. H.-C. Liu and A. Yariv, "Synthesis of high-order bandpass filters based on coupled resonator optical waveguides (CROWs)," Opt. Express **19**, 17653–17668 (2011).
7. J. Scheuer and A. Yariv, "Sagnac effect in coupled-resonator slow-light waveguide structures," Phys. Rev. Lett. **96**, 053901 (2006).
8. M. A. Terrel, M. J. F. Digonnet, and S. Fan, "Performance limitation of a coupled resonant optical waveguide gyroscope," J. Lightwave Technol. **27**, 47–54 (2009).
9. B. Z. Steinberg, J. Scheuer, and A. Boag, "Rotation-induced superstructure in slow-light waveguides with mode degeneracy: optical gyroscopes with exponential sensitivity," J. Opt. Soc. Am. B **24**, 1216–1224 (2007).
10. C. Sorrentino, J. Toland, and C. P. Search, "Ultra-sensitive chip scale Sagnac gyroscope based on periodically modulated coupling of a coupled resonator optical waveguide," Opt. Express **20**, 354–363 (2012).
11. J. R. E. Toland, Z. A. Kaston, C. Sorrentino, and C. P. Search, "Chirped area coupled resonator optical waveguide gyroscope," Opt. Lett. **36**, 1221–1223 (2011).
12. R. Novitski, B. Z. Steinberg, and J. Scheuer, "Losses in rotating degenerate cavities and a coupled-resonator optical-waveguide rotation sensor," Phys. Rev. A **85**, 023813 (2012).
13. M. Terrel, M. J. F. Digonnet, and S. Fan, "Performance comparison of slow-light coupled-resonator optical gyroscopes," Laser Photon. Rev. **3**, 452–465 (2009).
14. D. Hah and D. Zhang, "Analysis of resonant optical gyroscopes with two input/output waveguides," Opt. Express **18**, 18200–18205 (2010).
15. J. R. E. Toland and C. P. Search have prepared a manuscript titled, "Sagnac gyroscope using a two dimensional array of coupled optical microresonators," Phys. Rev. A (to be published).
16. C. Ciminelli, F. Dell'Olio, C. E. Campanella, and M. N. Armenise, "Photonic technologies for angular velocity sensing," Adv. Opt. Photon. **2**, 370–404 (2010).
17. J. Capmany, P. Munoz, J. D. Domenech, and M. A. Muriel, "Apodized coupled resonator waveguides," Opt. Express **15**, 10196–10206 (2007).
18. J. K. S. Poon, J. Scheuer, S. Mookherjea, G. T. Paloczi, Y. Huang, and A. Yariv, "Matrix analysis of microring coupled-resonator optical waveguides," Opt. Express **12**, 90–103 (2004).
19. J. K. S. Poon, J. Scheuer, Y. Xu, and A. Yariv, "Designing coupled-resonator optical waveguide delay lines," J. Opt. Soc. Am. B **21**, 1665–1673 (2004).
20. C. P. Search, J. R. E. Toland, and M. Zivkovic, "Sagnac effect in a chain of mesoscopic quantum rings," Phys. Rev. A **79**, 053607 (2009).
21. L.-W. Luo, G. S. Wiederhecker, J. Cardenas, C. Poitras, and M. Lipson, "High quality factor etchless silicon photonic ring resonators," Opt. Express **19**, 6284–6288 (2011).